

Collisionally inhomogeneous Bose-Einstein condensates in double-well potentials

C. Wang,¹ P.G. Kevrekidis,¹ N. Whitaker,¹ D. J. Frantzeskakis,² P. Schmelcher,^{3,4} and S. Middelkamp³

¹*Department of Mathematics and Statistics, University of Massachusetts, Amherst MA 01003-4515, USA*

²*Department of Physics, University of Athens, Panepistimiopolis, Zografos, Athens 157 84, Greece*

³*Theoretische Chemie, Physikalisches-Chemisches Institut,*

Im Neuenheimer Feld 229, Universität Heidelberg, 69120 Heidelberg, Germany

⁴*Physikalisches Institut, Universität Heidelberg, Philosophenweg 12, 69120 Heidelberg, Germany*

In this work, we consider quasi-one-dimensional Bose-Einstein condensates (BECs), with spatially varying collisional interactions, trapped in double well potentials. In particular, we study a setup in which such a “collisionally inhomogeneous” BEC has the same (attractive-attractive or repulsive-repulsive) or different (attractive-repulsive) type of interparticle interactions. Our analysis is based on the continuation of the symmetric ground state and anti-symmetric first excited state of the non-interacting (linear) limit into their nonlinear counterparts. The collisional inhomogeneity produces a saddle-node bifurcation scenario between two additional solution branches; as the inhomogeneity becomes stronger, the turning point of the saddle-node tends to infinity and eventually only the two original branches remain present, which is completely different from the standard double-well phenomenology. Finally, one of these branches changes its monotonicity as a function of the chemical potential, a feature especially prominent, when the sign of the nonlinearity changes between the two wells. Our theoretical predictions, are in excellent agreement with the numerical results.

I. INTRODUCTION

The remarkable progress in the experimental and theoretical studies of Bose-Einstein condensates (BECs) [1, 2] over the past two decades has sparked an intense study of the coherent nonlinear structures that arise in this setting. Such structures are rather naturally expected to emerge due to a well-established mean-field description of BECs by the Gross-Pitaevskii (GP) equation, namely, a nonlinear Schrödinger (NLS) equation, in which the nonlinearity is introduced by the interatomic interactions. This feature has inspired many relevant theoretical and experimental studies devoted to macroscopic nonlinear matter waves, such as bright matter-wave solitons in attractive BECs [3, 4, 5], as well as dark [6, 7, 8, 9] and gap [10] matter wave solitons in repulsive BECs (see also the recent review [11]). One of the important elements of the versatility of this atomic physics setting is the existence of diverse types of external potentials in the GP equation accounting for the electric, magnetic, optical or combined confinement of ultracold dilute alkali vapors that constitute the BEC. Some of the most typical forms of such trapping potentials include a parabolic and a spatially periodic one (created by the interference of counter-propagating laser beams, the so-called optical lattice). The NLS equations with similar potentials are also relevant in the context of nonlinear optics, where they model the evolution of optical beams in graded-index waveguides and periodic waveguiding arrays [12, 13].

One interesting type of potential that has drawn a considerable amount of attention is the double-well potential. This may originate, for instance, from the combination of a parabolic with a periodic potential. Its experimental realization was featured in Ref. [14], where a variety of interesting phenomena were studied; these include Josephson oscillations and tunneling for a small number of atoms, or macroscopic quantum self-trapping and an asymmetric partition of the atoms between the wells for sufficiently large numbers of atoms. In parallel to these experimental findings, numerous theoretical insights on this topic have emerged [15, 16, 17, 18, 19, 20, 21, 22, 23]. These concerned finite-mode reductions, analytical results for specially designed shapes of the potential, quantum depletion effects, and other theoretical aspects. Interestingly, double-well potentials have also been studied in applications arising in the context of nonlinear optics, including twin-core self-guided laser beams in Kerr media [24], optically induced dual-core waveguiding structures in a photorefractive crystal [25], trapped light beams in a structured annular core of an optical fiber [26], and so on. It is relevant to point out here that double well settings have been examined not only in one-component systems, but also in multi-component cases. In particular, a recent study motivated by two-component BECs can be found in [27], while similar attempts have been made in the context of the so-called spinor BECs (where it is possible to have three, and even five components) in the works of [28, 29]. These works examined not only finite-mode reductions of the multi-component case, but also phenomena beyond the level of the mean-field description such as quantum entanglement and spin-squeezing properties.

On the other hand, nonlinear matter-waves have not only been studied in a variety of external potentials, but also in the presence of temporally or spatially varying external fields manipulating the interatomic interactions. Indeed, the s-wave scattering length (which characterizes the nonlinearity coefficient in the GP equation) can be adjusted experimentally by employing either magnetic [30, 31] or optical Feshbach resonances [32] in a very broad range. This flexibility of manipulation of the interatomic interactions has motivated a significant number of studies both on the theoretical and on the experimental front; in particular, on the experimental side, the formation of bright matter-wave

solitons and soliton trains for ${}^7\text{Li}$ [3, 4] and ${}^{85}\text{Rb}$ [5] atoms used a tuning of the interatomic interactions from repulsive to attractive. Also, this type of manipulations was instrumental in achieving the formation of molecular condensates [33], and the probing of the BEC-BCS crossover [34]. On the other hand, theoretical studies have predicted that a time-dependent modulation of the scattering length can be used to stabilize attractive higher-dimensional BECs against collapse [35], or to create robust matter-wave breathers in lower-dimensional BECs [36]. While the above studies focused on temporal variations of the interaction strength, more recently spatial variations of the nonlinearity have come to be of interest in the so-called ‘‘collisionally inhomogeneous’’ environments. These have been found to lead to a variety of interesting developments including (but not limited to) adiabatic compression of matter-waves [37, 38], Bloch oscillations of matter-wave solitons [37], atomic soliton emission and atom lasers [39], enhancement of transmittivity of matter-waves through barriers [40, 41], dynamical trapping of matter-wave solitons [40], stable condensates exhibiting both attractive and repulsive interatomic interactions [42], the delocalization transition of matter waves [43], and so on. Many different types of spatial variations of the nonlinearity have been considered, including linear [37, 40], parabolic [44], random [45], periodic [43, 46, 47], and localized (step-like) [39, 48, 49] ones. Furthermore, a number of detailed mathematical studies [50, 51, 52] have appeared, addressing aspects such as the effect of a ‘‘nonlinear lattice potential’’ (i.e., a spatially periodic nonlinearity) on the stability of matter-wave solitons, and the interplay between drift and diffraction/blow-up instabilities. More recently, the interplay of nonlinear and linear potentials has been examined in both continuum [53] and discrete [54] settings.

The aim of the present work is, in fact, to combine these two interesting settings, namely the double-well potential and a collisionally inhomogeneous (i.e., spatially dependent) nonlinearity. As, arguably, one of the simplest forms of this combination, we select a coefficient of the nonlinearity which is piecewise constant, in line with the suggestions of [39, 49, 55] and can vary between two (smoothly connected) pieces with the same sign, or even two pieces with opposite signs. The latter form of a spatially dependent nonlinearity appears to be one that should be straightforwardly experimentally realizable [56], through the use of magnetic field gradients of moderate size for atom chips (see also the relevant discussion in [55]). The phenomenology that we observe in this setting appears to be *remarkably different* from that of the standard double-well. In particular, as we detailed in an earlier relevant work [22], the linear states of the underlying potential can be continued into nonlinear ones in the presence of the pertinent cubic nonlinearity. As prototypical examples of these linear states one can consider the symmetric ground state and the anti-symmetric first excited state of the double-well potential. A remarkable feature, however, which takes place for sufficiently strong nonlinearity (to the symmetric state for attractive interactions and to the anti-symmetric state for repulsive interactions) is a symmetry-breaking bifurcation of the pitchfork type. This bifurcation generates two new asymmetric solutions (which exist for sufficiently large nonlinearity). What we find here is that even a weak inhomogeneity in the collisional properties of the condensate changes the nature of this bifurcation from a pitchfork to a saddle-node one. This may be anticipated given the ‘‘non-parametrically robust’’ nature of the pitchfork bifurcation which will yield similar changes in the presence of different asymmetries (see also [22]). In addition to that, increasing the inhomogeneity strength shifts (eventually to infinity) the turning point of the saddle-node bifurcation. Thus, for sufficiently large variation of the nonlinear coefficient between the two wells, only two nonlinear states emanate from the ground and first excited states of the linear problem. Furthermore, for one of these states, the monotonicity of the number of particles changes as a function of its nonlinear eigenvalue parameter (i.e., the chemical potential). This is a rather unusual feature that leads to a bifurcation diagram entirely different from those of the homogeneous interatomic interactions (i.e., homogeneous nonlinearity) limit of either the one-component [22] or of the multi-component system (see e.g., [27]).[63] These traits are captured accurately, as we will show below, by a two-mode, Galerkin-type approximation [21, 22] applied to the present collisionally inhomogeneous double well setting.

Our presentation is structured as follows. The model and the semi-analytical predictions regarding its stationary solutions are presented in section II. Our corresponding directly numerical findings and their comparison with the analysis are given in section III. In section IV, we present an alternative theoretical viewpoint more akin to the model dynamics and compare its results to the full results of the partial differential equation. Finally, in section V, we present our summary and conclusions.

II. THE MODEL AND ITS SEMI-ANALYTICAL CONSIDERATION

The dynamics of a quasi one-dimensional (1D) condensate, oriented along the x -axis, can be described by the following GP equation (see, e.g., Ch. 1 in [11] and [57]),

$$i\hbar\partial_t\Psi = \left(-\frac{\hbar^2}{2m} + V(x) + g|\Psi|^2 - \mu \right) \Psi, \quad (1)$$

where $\Psi(x, t)$ is the mean-field order parameter, m is the atomic mass, and μ is the chemical potential of the effectively 1D system. The nonlinear coefficient g arises from the interatomic interactions and has an effective 1D form, namely

$g = 2\hbar\omega_{\perp}a$, where ω_{\perp} is the transverse confining frequency and a is the three-dimensional (3D) s-wave scattering length (the cases $a > 0$ or $a < 0$ correspond, respectively, to repulsive or attractive interatomic interactions). The external potential $V(x)$ in the GP Eq. (1) consists of a regular harmonic trap and a repulsive potential localized at the harmonic trap center, namely,

$$V(x) = \frac{1}{2}m\omega_x^2x^2 + V_0\text{sech}^2\left(\frac{x}{w_B}\right), \quad (2)$$

where ω_x is the longitudinal confining frequency, while V_0 and w_B are, respectively, the strength and width of the localized potential; the latter is in fact a barrier potential that may be created by a blue-detuned laser beam, repelling the atoms in the condensate. It is clear that the combination of the harmonic trap and the barrier potential is in fact a double-well potential.

Moreover, we assume that the collisional properties of the condensate are spatially inhomogeneous, i.e., $a = a(x)$, with the function $a(x)$ taking different, but smoothly connected, values in the two wells of the external potential. In particular, we consider that an external magnetic or optical field (see below) modifies the scattering length of the condensate as follows,

$$a(x) = a_0 + a_1 \tanh\left(\frac{x}{W}\right), \quad (3)$$

where a_0 and a_1 are constant values of the condensate's scattering length in the absence and in the presence of the external field, respectively, which are smoothly connected through the tanh function (here, W is the spatial length scale on which the transition between the two values a_0 and a_1 takes place). Apparently, far away from the harmonic trap center at $x = 0$ (or, in other words, far away from the barrier), the scattering length takes the values $a = a_0 \pm a_1$, for $x \rightarrow \pm\infty$ respectively. Such an inhomogeneity of the scattering length may be realized in practice upon employing a bias homogeneous field and imposing a steep localized gradient on top of it. In such a case, in a quasi 1D configuration (as is the case under consideration) this will lead to a constant scattering length with value $a = a_1$ in the left well, which is followed by a localized change of a , finally ending up with a second value $a = a_2$ in the right well. Notice that in our model we choose the function tanh to analytically describe the transition between these different constant values of a since there are no ideal steps, but rather close approximations to it. Also, we naturally assume that we are relatively close to a Feshbach resonance, in order to easily manipulate the scattering length with the external field.

Next, measuring time in units of the inverse transverse trapping frequency ω_{\perp}^{-1} , length in units of the transverse oscillator length $l_{\perp} \equiv \sqrt{\hbar/m\omega_{\perp}}$, energy in units of $\hbar\omega_{\perp}$, and introducing the normalized wavefunction $u(x, t) = (2|a_r|)^{1/2}\Psi(x, t)$ (where a_r is a reference value of the scattering length), we reduce the GP Eq. (1) to the following dimensionless form:

$$i\partial_t u = Hu + \Gamma(x)|u|^2u - \mu u. \quad (4)$$

In the above equation,

$$H \equiv -\frac{1}{2}\partial_x^2 + V(x) \quad (5)$$

is the "single-particle" operator in the normalized external potential

$$V(x) = \frac{1}{2}\Omega^2x^2 + V_0\text{sech}^2\left(\frac{x}{w}\right), \quad (6)$$

with $\Omega \equiv \omega_x/\omega_{\perp}$ being the normalized harmonic trap strength and $w = w_B/l_{\perp}$. The nonlinearity coefficient $\Gamma(x)$ in Eq. (4) is given by

$$\Gamma(x) = \alpha + \beta \tanh(bx), \quad (7)$$

where $\alpha = a_1/|a_r|$, $\beta = a_2/|a_r|$, and $b = l_{\perp}/W$. Apparently, the cases $\Gamma > 0$ or $\Gamma < 0$ correspond to repulsive or attractive interactions, respectively. We finally mention that the number of particles in the condensate \mathcal{N} is now defined as $\mathcal{N} = (l_{\perp}/2|a_r|)N$, where

$$N = \int_{-\infty}^{+\infty} |u(x, t)|^2 dx \quad (8)$$

is an integral of motion (normalized number of particles) of the GP Eq. (4). Also, in our analysis (and particularly in the typical numerical results that will be presented below) we will assume fixed parameter values $\Omega = 0.1$, $V_0 = 1$, $w = 0.5$ and $b = 1$.

In the non-interacting limit [i.e., for $\Gamma(x) = 0$], the spectrum of the underlying linear Schrödinger equation consists of a ground state, $u_0(x)$, and excited states, $u_l(x)$ ($l \geq 1$). Our analytical investigation of the nonlinear problem (at the stationary level) in the weakly nonlinear regime consists of applying a Galerkin-type, two-mode approximation to Eq. (4). In particular, we assume that the wavefunction $u(x, t)$ can be decomposed as

$$u(x, t) = c_0(t)u_0(x) + c_1(t)u_1(x), \quad (9)$$

where $c_0(t)$ and $c_1(t)$ are unknown time-dependent complex prefactors. Substituting Eq. (9) into Eq. (4) and projecting the resulting equation to eigenfunctions u_0 and u_1 , we obtain the following equations:

$$i\dot{c}_0 = (\omega_0 - \mu)c_0 + A_0|c_0|^2c_0 + D_0(2|c_0|^2c_1 + c_0^2c_1^*) + B(2|c_1|^2c_0 + c_1^2c_0^*) + D_1|c_1|^2c_1, \quad (10)$$

$$i\dot{c}_1 = (\omega_1 - \mu)c_1 + A_1|c_1|^2c_1 + D_1(2|c_1|^2c_0 + c_1^2c_0^*) + B(2|c_0|^2c_1 + c_0^2c_1^*) + D_0|c_0|^2c_0. \quad (11)$$

In these equations, dots denote time derivatives, stars denote complex conjugates, and $\omega_{0,1}$ are the eigenvalues corresponding to the eigenstates $u_{0,1}$; in the numerical examples presented herein, ω_0 and ω_1 can be numerically found to be 0.133 and 0.156 respectively. We should note in passing here that although $\omega_{0,1}$ and $u_{0,1}$ are numerically obtained through a simple eigensolver of the underlying linear Schrödinger problem, it is also, in principle, possible to develop a perturbative approach towards obtaining such eigenvalues and eigenvectors following the work of [58], rendering our semi-analytical approach developed below more proximal to a fully analytical one. The overlap integrals $A_0 = \int \Gamma(x)u_0^4(x)dx$, $A_1 = \int \Gamma(x)u_1^4(x)dx$, $B = \int \Gamma(x)u_0^2(x)u_1^2(x)dx$, $D_0 = \int \Gamma(x)u_0^3(x)u_1(x)dx$ and $D_1 = \int \Gamma(x)u_0(x)u_1^3(x)dx$ are constants. Notice that $u_0(x)$ and $u_1(x)$ are both real functions (due to the Hermitian nature of the underlying linear Schrödinger problem) and are also orthonormal. In what follows, in the definition of $\Gamma(x)$ in Eq. (7), we will set

$$\alpha + \beta = -1, \quad \alpha - \beta = -1 + \varepsilon, \quad (12)$$

with $0 \leq \varepsilon \leq 2$, as shown in Fig. 1. Notice that in the limiting case $\varepsilon = 0$, the nonlinearity coefficient takes a constant value, $\Gamma(x) = -1$, and the problem is reduced to the study of a collisionally homogeneous condensate with attractive interatomic interactions in a double well potential; this problem was studied in detail in Ref. [22] by means of the considered two-mode approximation for both symmetric and asymmetric double-well potentials. As a result of this choice and of fixing the rest of the parameters, the above overlap integrals A_0 , A_1 , B , D_0 and D_1 are functions of ε and their dependence on this parameter is shown in Fig. 2.

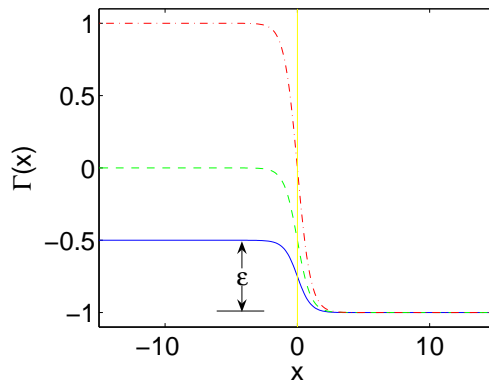


FIG. 1: The nonlinearity coefficient $\Gamma(x) = \alpha + \beta \tanh(bx)$ with parameters $\alpha + \beta = -1$, $\alpha - \beta = -1 + \varepsilon$, and $b = 1$. The figure displays some examples of the shape of $\Gamma(x)$ for different values of ε (i.e., the inhomogeneity parameter): $\varepsilon = 0.5$ (blue solid line), $\varepsilon = 1$ (green dashed line) and $\varepsilon = 2$ (red dashed-dotted line).

We now introduce in Eqs. (10)-(11) the amplitude-phase variables $c_j = \rho_j e^{i\varphi_j}$, $j = 0, 1$ (the functions ρ_j and φ_j are assumed to be real and are time-dependent) and derive from Eqs. (10) and (11) the equations for ρ_0 and φ_0 :

$$\dot{\rho}_0 = B\rho_0\rho_1^2 \sin(2\varphi) + (D_0\rho_0^2\rho_1 + D_1\rho_1^3) \sin(\varphi), \quad (13)$$

$$\dot{\varphi}_0 = (\mu - \omega_0) - A_0\rho_0^2 - B(2\rho_1^2 + \rho_1^2 \cos(2\varphi)) - (3D_0\rho_0\rho_1 + D_1\frac{\rho_1^3}{\rho_0}) \cos(\varphi), \quad (14)$$

where $\varphi = \varphi_0 - \varphi_1$ is the relative phase between the two modes. The equations for ρ_1 and φ_1 can directly be obtained by interchanging indices 1 and 0 in Eqs. (13) and (14).

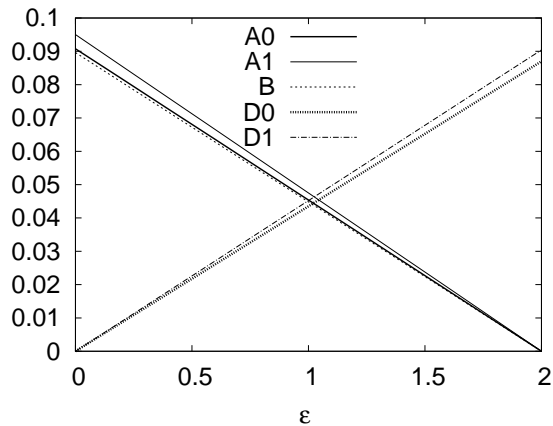


FIG. 2: The dependence of the overlap integrals A_0 , A_1 , B , D_0 and D_1 on ϵ (for our choice of the rest of the parameters of the potential and of $\Gamma(x)$).

Focusing on real solutions of Eq. (4), we consider the steady solutions, i.e., $\dot{\rho}_0 = \dot{\varphi}_0 = 0$ [associated to the fixed points of the dynamical system of Eqs. (13)-(14)], with $\varphi = k\pi$ with k an integer. In such a case, the equations for ρ_0 [Eq. (13)] and ρ_1 are automatically satisfied, while the equations for φ_0 [Eq. (14)] and φ_1 are reduced to the following algebraic system:

$$(\mu - \omega_0) - A_0\rho_0^2 - 3B\rho_1^2 - 3D_0\rho_0\rho_1 - D_1\frac{\rho_1^3}{\rho_0} = 0, \quad (15)$$

$$(\mu - \omega_1) - A_1\rho_1^2 - 3B\rho_0^2 - 3D_1\rho_1\rho_0 - D_0\frac{\rho_0^3}{\rho_1} = 0. \quad (16)$$

The semi-analytical part of our considerations will consist of solving these algebraic conditions for given linear potential $V(x)$ and nonlinear spatial dependence $\Gamma(x)$ parameters (as mentioned above) and we will compare the findings from this two-mode, Galerkin-type truncation with the full numerical results in what follows.

It is interesting to briefly address the case where $\phi \neq k\pi$ (hence $n(\phi) \neq 0$). In that case, the stationary form of Eq. (13) leads to:

$$\cos(\phi) = -\frac{D_0\rho_0^2 + D_1\rho_1^2}{2B\rho_0\rho_1}. \quad (17)$$

Then it is straightforward to observe that since $D_0 < D_1$, for all ϵ , and $B < D_1$ for $\epsilon > 0.995$ (from Fig. 2), for such values of ϵ , the fraction of the right-hand-side of Eq. (17) can be shown to be < -1 and, hence, there are no other solutions satisfying Eq. (13). For $\epsilon < 0.995$ we could not perform a similar semi-analytical calculation. However, we confirmed numerically the non-existence of additional solutions (to the ones with $\phi = k\pi$) for this domain.

III. NUMERICAL RESULTS

We begin the exposition of our numerical results by considering $0 < \epsilon < 1$, in which case $\Gamma(x) < 0$, i.e., attractive interatomic interactions. The top panels of Fig. 3 show two examples: $\epsilon = 0.25$ (left) and $\epsilon = 0.5$ (right). Each of these panels presents the complete diagram of the numerically generated solutions (blue solid lines correspond to stable solutions and red dashed lines to unstable ones) to Eq. (4) and the corresponding analytical predictions (green dashed-dotted lines), namely, the results of the two mode approximation obtained by solving Eqs. (15) and (16). The solutions are expressed in terms of the normalized number of atoms N [see Eq. (8)] as a function of the normalized chemical potential μ . The branches are obtained using a fixed-point Newton iteration and numerical continuation from the non-interacting limit of the system (i.e., in the absence of nonlinearity). Then, numerical linear stability analysis is performed to determine whether each branch does or does not possess real eigenvalues (which result in instability). It is readily observed that the analytical predictions for the different branches through Eqs. (15)-(16) are in very good agreement with the numerically found solutions.

Let us now discuss the various branches appearing in the bifurcation diagrams in more detail. Branch I corresponds to the asymmetric (due to the collisional inhomogeneity) solution starting at $\mu = \omega_0$, the eigenvalue corresponding

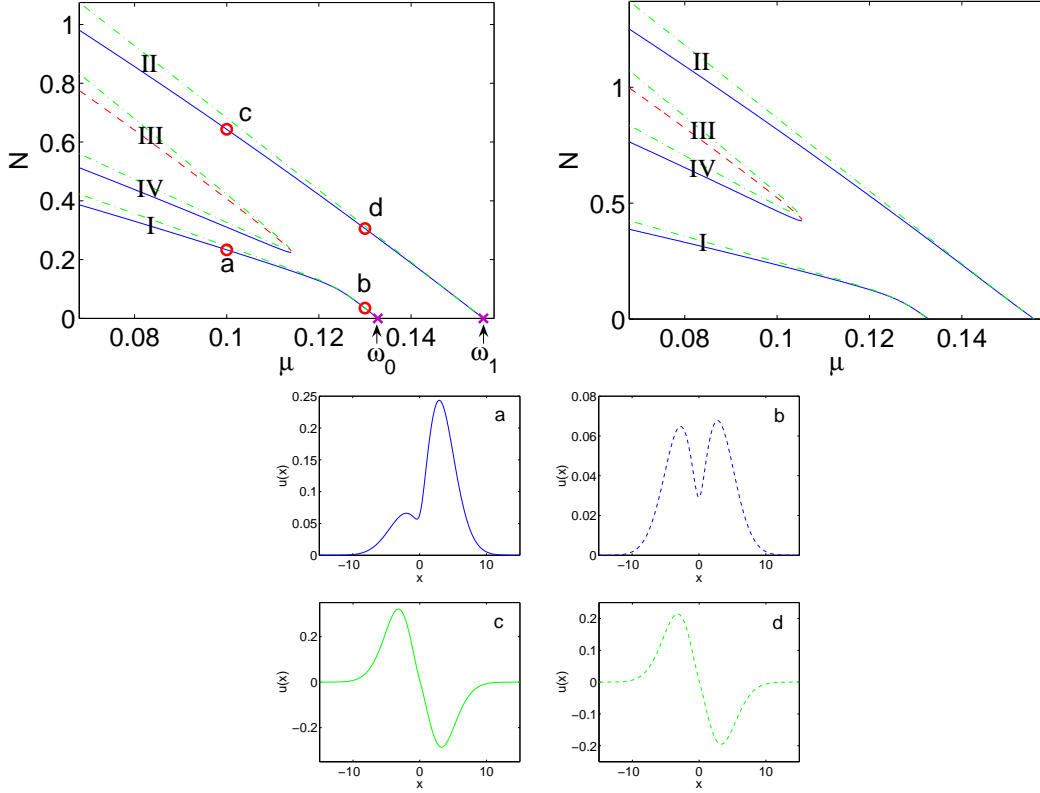


FIG. 3: Top panels: The normalized number of atoms N [see Eq. (8)] of the solutions of Eq. (4) for the case of attractive interatomic interactions i.e., for a nonlinearity coefficient $\Gamma(x)$ with parameters $\alpha + \beta = -1$ and $\alpha - \beta = -1 + \varepsilon$, with $\varepsilon = 0.25$ (top left) and $\varepsilon = 0.5$ (top right), as a function of the normalized chemical potential μ . The blue solid lines and red dashed lines denote the stable and unstable numerically found solutions. The green dashed-dotted lines depict the result of the two-mode approximation. Notice that as $N \rightarrow 0$, the spatial profiles of the two branches tend to the linear eigenmodes $u_{0,1}$ and accordingly $\mu \rightarrow \omega_{0,1}$. Bottom panels: The profiles of the wave functions corresponding to branch I (upper blue) and II (lower green). Along each branch, the profiles are shown for two values of μ , i.e., $\mu = 0.1$ (left solid) and $\mu = 0.13$ (right dashed); the corresponding labels are a) and b) for the symmetric (in the linear limit) branch shown above, while c) and d) are for the antisymmetric (in the linear limit) branch shown below.

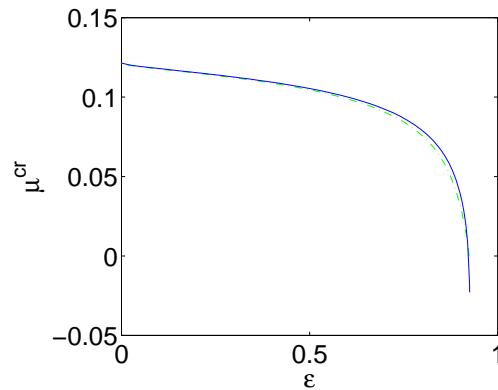


FIG. 4: The value of μ at which branches III and IV disappear as a function of ε with respect to Fig. 3. The blue solid lines and the green dashed-dotted lines denote the numerically found solutions and the result of the two-mode approximation, respectively.

to the symmetric ground eigenstate u_0 . The asymmetry arises immediately after the deviation from the linear limit of $N \rightarrow 0$, and becomes increasing as one drifts further away. Similarly, branch II starts from $\mu = \omega_1$, the eigenvalue of the anti-symmetric first excited eigenstate, and becomes increasingly asymmetric as it gets away from its linear limit, i.e., when N gets larger. The four bottom panels of Fig. 3 provide specific examples of the profiles of this continuation.

Branches III and IV correspond to a pair of two other asymmetric solutions which collide at some critical value of $\mu \equiv \mu^{cr}$ and disappear from then on through a saddle-mode bifurcation. As for the two examples in Fig. 3, the critical points are 0.1140 and 0.1054, for the cases $\varepsilon = 0.25$ and $\varepsilon = 0.5$, respectively. Moreover, branch IV is observed to move towards branch I as $\varepsilon \rightarrow 0$. Specifically, when $\varepsilon = 0$, branch IV merges into branch I and the diagram turns into a pitchfork bifurcation (the two asymmetric branches are mirror images of each other and both bifurcate from the symmetric solution in that case), which is the case with attractive interactions analyzed in Ref. [22]. As ε increases, the critical point μ^{cr} of the saddle-node bifurcation decreases and tends to negative infinity rapidly, especially as ε gets closer to 1; then, branches III and IV keep moving to the left of the diagram and disappear finally when ε is close enough to 1. Also, the stability analysis indicates that branch III is the only unstable one among the four solutions, while the other three are all stable for any value of μ .

As a stringent test of our analytical two-mode approximation, in Fig. 4 we show the critical point of the saddle-node bifurcation μ^{cr} as a function of the collisional inhomogeneity parameter ε . We observe that the solid line of the fully numerical results is almost identical to the dashed line yielding the theoretical prediction for the occurrence of this bifurcation. This figure demonstrates excellent agreement between the analytical results and the numerical findings.

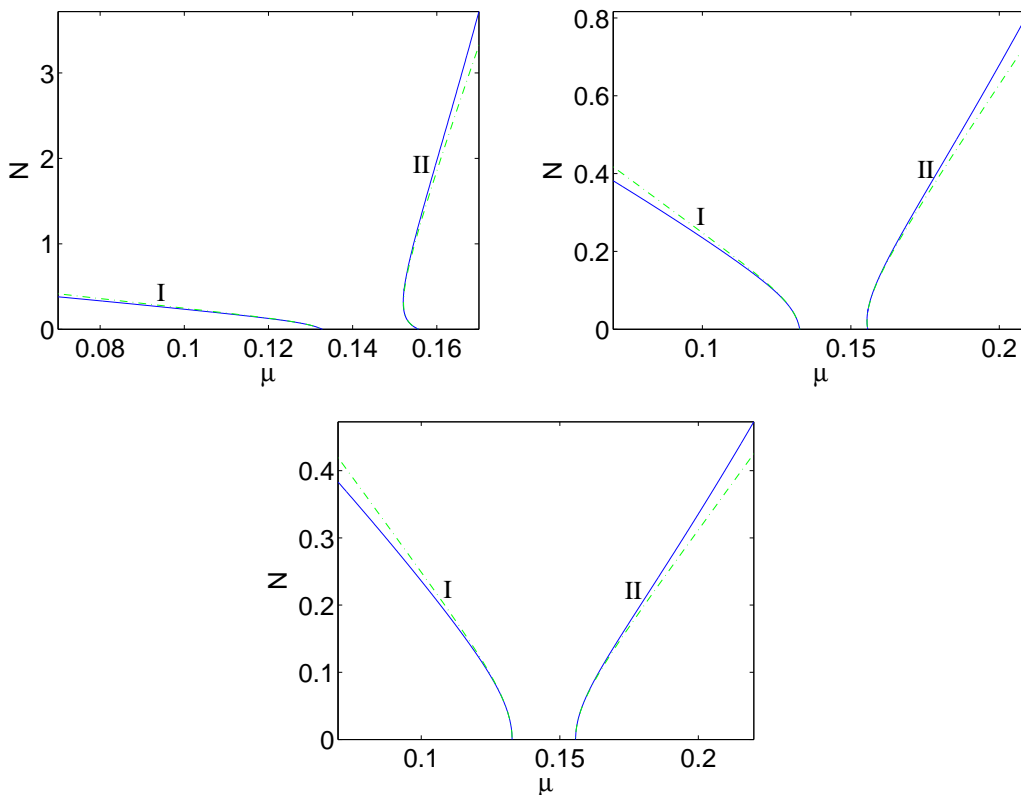


FIG. 5: The norm of the solutions of Eq. (4) for a nonlinearity coefficient $\Gamma(x)$ with parameters such that $\alpha + \beta = -1$ and $\alpha - \beta = -1 + \varepsilon$, with $\varepsilon = 1.05$ (top left), $\varepsilon = 1.5$ (top right) and $\varepsilon = 2$ (bottom), as a function of μ . The notation is the same as in Fig. 3.

Next, we study the behavior of the solutions when $\varepsilon > 1$, in which case the nonlinearity is no longer purely attractive. Remarkably, in this case, only two solutions, branch I and II, still survive for all the examined values of $\varepsilon > 1$. We realize that when ε grows larger from 0 to 1, both branches I and II move 'clockwise' and branch II appears to be almost vertical when ε passes the value 1. As ε continues to increase from 1 to 2, we find an interesting new phenomenon: within a certain small range of N , the solution II only exists for chemical potentials μ slightly less than the eigenvalue ω_1 (corresponding to the eigenstate u_1) before it meets a turning point; the latter occurs, for example, at $\mu = 0.1520$ or 0.1554 for the cases $\varepsilon = 1.05$ or 1.5 , respectively. After the turning point, the solution exists when

μ gets larger. This phenomenon is shown in Fig. 5, in which it is observed that branch II starts at the linear limit, persists with $dN/d\mu < 0$ for a narrow interval of chemical potentials, before turning to the right with and acquiring $dN/d\mu > 0$. It is also worth mentioning that both branches I and II are still asymmetric and *stable* in this case; thus, here we observe an interesting deviation from the well-known Vakhitov-Kolokolov criterion [59] (see, e.g., a relevant discussion in Ref. [60]) about the slope of the branch determining its linear stability. We present an explanation of the relevant feature at the end of this section (after observing similar features in the principally defocusing case below).

Now let us consider the case in which the parameters involved in the nonlinearity coefficient $\Gamma(x)$ are such that

$$\alpha + \beta = 1 - \varepsilon, \quad \alpha - \beta = 1, \quad (18)$$

with $0 \leq \varepsilon \leq 2$, as shown in Fig. 6. Notice that Eqs. (12) and (18) produce the same results when $\varepsilon = 2$.

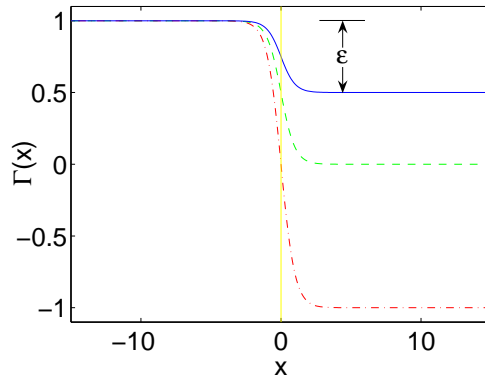


FIG. 6: Similar to Fig. 1, but with a nonlinearity coefficient $\Gamma(x)$ such that $\alpha + \beta = 1 - \varepsilon$, $\alpha - \beta = 1$ and $b = 1$, with $\varepsilon = 0.5$ (blue solid line), $\varepsilon = 1$ (green dashed line) and $\varepsilon = 2$ (red dashed-dotted line).

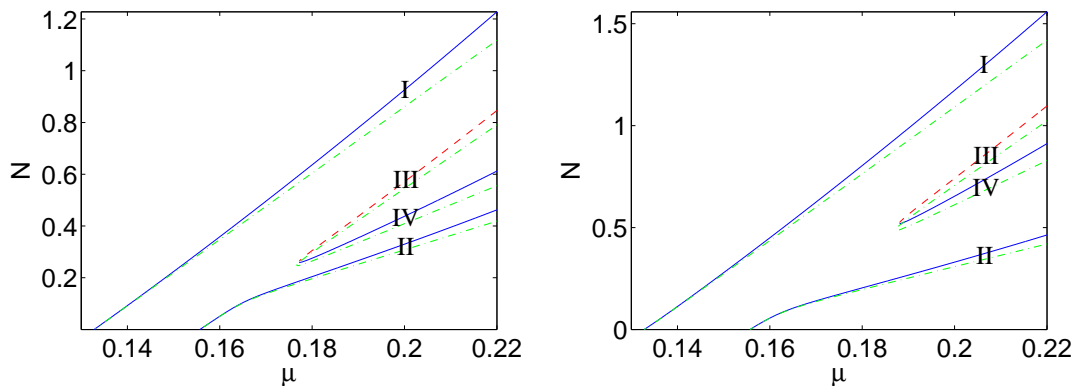


FIG. 7: The normalized number of particles N for the solutions of Eq. (4) as a function of μ in the case of repulsive interatomic interactions, namely, for a nonlinearity coefficient $\Gamma(x)$ with parameters such that $\alpha + \beta = 1 - \varepsilon$ and $\alpha - \beta = 1$, with $\varepsilon = 0.25$ (left) and $\varepsilon = 0.5$ (right). The notation is the same as in Fig. 3.

Figure 7 shows some prototypical examples of the bifurcation diagram of the relevant solutions when $0 < \varepsilon < 1$, i.e., in the case of a purely repulsive nonlinearity (notice that the branches turn to the opposite direction than in Fig. 3). Similar to the previous case, four solutions are found, two of which disappear through a saddle node bifurcation, allowing only two to survive in the non-interacting (linear) limit of $N \rightarrow 0$. As before, the saddle-node bifurcation becomes a pitchfork one (but now emerging from the anti-symmetric branch) in the case of a collisionally homogeneous environment i.e., for $\varepsilon \rightarrow 0$. Preserving the original notations, branches I and II are the two asymmetric solutions extending to the linear limit, and starting at $\mu = \omega_0$ and $\mu = \omega_1$, respectively. Once again branches III and IV disappear when μ decreases to some critical value μ^{cr} , which goes up to infinity as ε increases to 1. The dependence of μ^{cr} on the inhomogeneity parameter ε is shown in Fig. 8. It is important once again to highlight the good

qualitative and even quantitative (apart from the case of very large ε) agreement of the two-mode prediction for μ^{cr} with the full numerical results.

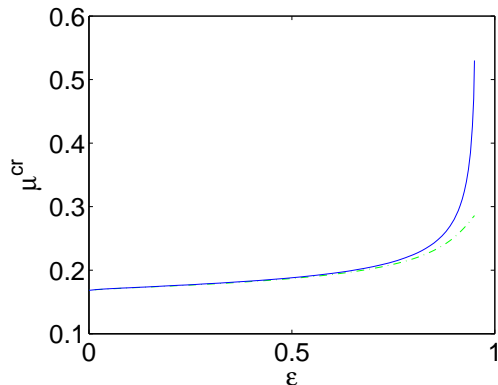


FIG. 8: The critical value μ^{cr} of the normalized chemical potential at which branches III and IV disappear as a function of ε with respect to Fig. 6. The blue solid lines and the green dashed-dotted lines denote the numerically found solutions and the prediction of the two-mode approximation, respectively.

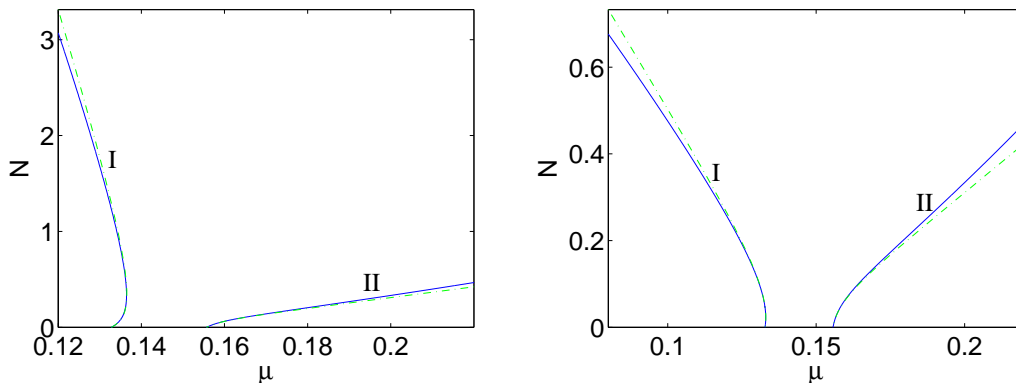


FIG. 9: The normalized number of particles N of the solutions of Eq. (4) as a function of μ , for a nonlinearity coefficient $\Gamma(x)$ with parameters such that $\alpha + \beta = 1 - \varepsilon$ and $\alpha - \beta = 1$, with $\varepsilon = 1.05$ (left) and $\varepsilon = 1.5$ (right), The notation is the same as in Fig. 3.

It is interesting to note that in this case as ε increases and one of the wells becomes less repulsive (and eventually attractive for $\varepsilon > 1$), the branches I and II keep rotating 'counterclockwise'. For $\varepsilon > 1$, the turning of the branch arises again, on branch I this time, as shown in Fig. 9. In this case, the bifurcation diagram contains only two branches which, for sufficiently large ε , feature opposite monotonicity of the dependence of N on the chemical potential μ (although both branches are linearly stable). Similarly to the previous case, branch III is the unstable solution, while the other three remain stable. In all the cases (and even these of large ε), we again note the strong agreement between the bifurcation diagram predicted by the two-mode approximation, in comparison with the numerical results.

We observe that in Fig. 5 (e.g., in its top left panel) for the case where the nonlinearity is principally focusing, as well as in Fig. 9 (e.g., in its left panel), where it is principally defocusing, one of the branches changes its monotonicity, as a result of the spatially dependent nonlinearity. As indicated previously, given the slope condition of the Vakhitov-Kolokolov criterion [59], it appears to be rather surprising that this change of monotonicity is not accompanied by a change of stability. However, we argue here that it is not. Defining the well known linearization operators

$$L_+ = -\frac{1}{2}\partial_x^2 + V(x) + 3g(x)|u|^2 - \mu \quad (19)$$

$$L_- = -\frac{1}{2}\partial_x^2 + V(x) + g(x)|u|^2 - \mu, \quad (20)$$

it is known from the work of [61] that when $|n(L_+) - n(L_-)| = 1$ [i.e., the number of negative eigenvalues of L_+

minus the negative eigenvalues of L_- is in absolute value equal to 1], instability arises when the slope condition of Vakhitov-Kolokolov is violated. Since, when $|n(L_+) - n(L_-)| > 1$, the relevant theory indicates that the solution is always unstable, we argue that what should be happening here is that the violation of the slope condition of Vakhitov-Kolokolov is not associated with an instability because it occurs at the same time as the change of the count of $|n(L_+) - n(L_-)|$ (from 1 to 0 or vice versa). This is precisely what we numerically illustrate in Fig. 10. In particular, the left panel concerns the principally focusing case associated to the first excited state “turning branch” of Fig. 5. There, given the fact that $n(L_-) = 1$ (due to the one zero-crossing of the configuration itself, which is an eigenfunction of L_- with a 0 eigenvalue), we expect the count of eigenvalues $n(L_+)$ to change from 2 to 1 exactly at the critical point, precisely as observed in the figure. On the other hand, the right panel concerning the ground state branch of Fig. 9 for the principally defocusing case, corresponds to a case with $n(L_-) = 0$. Hence, when the slope condition is violated (near the linear limit in this case), it has to be true that $n(L_+) = 0$, while after the turning point of the branch, the slope condition is satisfied and then $n(L_+) = 1$, which again is consonant with the observed stability. These features are clearly illustrated in the right panel of Fig. 10. We believe that similar considerations and counts may resolve apparent paradoxes that seem to be encountered e.g. in [60, 62].

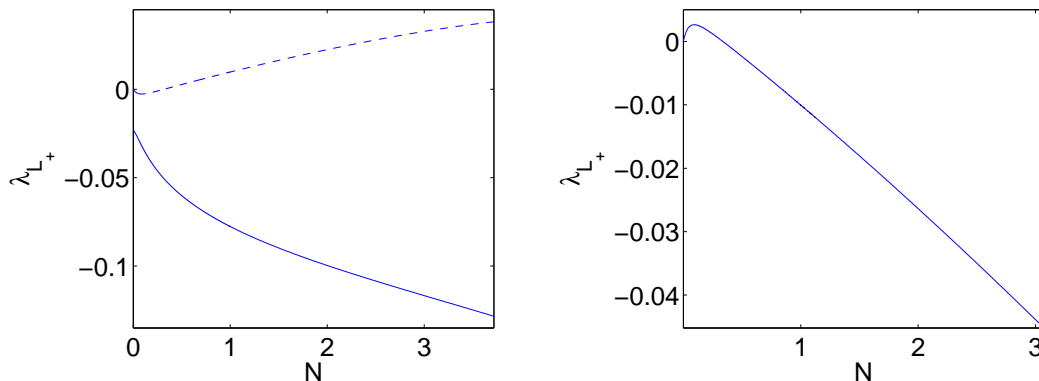


FIG. 10: The eigenvalues of the operator $L_+ = -\frac{1}{2}\partial_x^2 + V(x) + 3g|u|^2 - \mu$, which involve negative parts, as a function of N . The left and right panels relate to the two “turning branches”, i.e. branch II in Fig. 5 and branch I in Fig. 9, respectively, for the case that $\varepsilon = 1.05$.

IV. TWO-MODE DYNAMICS

So far, we have considered the two-mode reduction as a tool for identifying (quite successfully, as shown above) the stationary states of the underlying problem. However, here we illustrate how the same tool can be used to understand the system dynamics. The two principal dynamical features of the (symmetric) double well system involve the oscillations of matter between the two wells (for low population asymmetries between the wells) and the nonlinearly induced self-trapping regime (for high population asymmetries between the wells); see e.g., [15, 19]. For this reason, although our setting here is inherently asymmetric (due to the nature of $\Gamma(x)$), it is of interest to develop a variant of the two-mode approximation that accounts for the population imbalance between the wells.

In order to formulate the problem based on the populations of the left and right well, one can reformulate our two-mode decomposition as

$$u(x, t) = c_R(t) \frac{1}{\sqrt{2}}(u_0(x) + u_1(x)) + c_L(t) \frac{1}{\sqrt{2}}(u_0(x) - u_1(x)), \quad (21)$$

where it is clear that c_L and c_R are connected with c_0 and c_1 through a simple linear transformation. If we then decompose $c_i = \rho_i e^{i\phi_i}$ $i = R, L$ and define the phase difference $\Delta\phi = \phi_L - \phi_R$, and the population imbalance $z = \rho_R^2 - \rho_L^2$ (recall that $N = \rho_L^2 + \rho_R^2$), one can then project the equation to $(u_0 + u_1)$, as well as to $(u_0 - u_1)$ and

eventually obtain the dynamical equations for the conjugate variables z and $\Delta\phi$. These read:

$$\begin{aligned} \dot{\Delta\phi} = & -\frac{z}{4}(A_0 - 10B + A_1) + N(D_0 + D_1) - \cos(\Delta\phi)\frac{z}{\sqrt{N^2 - z^2}}\left(\mu_0 - \mu_1 + \frac{N}{2}(A_0 - A_1)\right) \\ & + \cos(\Delta\phi)\frac{N^2 - 2z^2}{\sqrt{N^2 - z^2}}(D_0 - D_1) - \cos(2\Delta\phi)\frac{z}{4}(A_0 - 2B + A_1) \end{aligned} \quad (22)$$

$$\dot{z} = \sqrt{N^2 - z^2}\sin(\Delta\phi)\left(\mu_0 - \mu_1 + \frac{N}{2}(A_0 - A_1) + z(B_0 - B_1)\right) + \frac{N^2 - z^2}{4}\sin(2\Delta\phi)(A_0 - 2B + A_1) \quad (23)$$

It is interesting to examine the dynamical evolution of these equations (their stationary states are identical to the ones identified above), and to compare their dynamics with the corresponding PDE dynamics. In the latter, one can also make similar projections to $(u_0 + u_1)$, as well as to $(u_0 - u_1)$ and define accordingly $c_{L,R}$, as well as thereafter z and $\Delta\phi$. A comparison of the $(z, \Delta\phi)$ phase space for different ϵ of such canonically conjugate variables can be found in Fig. 11. It can be clearly observed that for non-zero ϵ the reflection symmetry around $z = 0$ is broken. For increasing ϵ the population imbalance of the stationary states shifts towards larger values of z (see also Fig. 12), denoting a larger occupation of the right well compared to the left one. This can be understood by taking into account that we consider the case of repulsive interaction. There, an increase of ϵ implies a reduction of interaction in the right well (see Fig. 6). So, pictorially speaking, the atoms feel less repulsion in the right well than in the left one, leading to the observed population imbalance. For small populational asymmetries (around the nonzero stationary ones), the system executes inter-well matter-transfer oscillations. On the other hand, beyond a critical asymmetry in the initial populations, we enter the self-trapping regime, as is shown both in the partial differential equation of the full dynamics and in the above reduced two-mode description of Eqs. (22)-(23). For non-zero ϵ the value of this critical points taken at $\delta\phi = 0$ depend also on their sign, in contrary to the symmetric case for $\epsilon = 0$. For small values of ϵ there are two critical points, which increase with increasing ϵ . Eventually, the positive one ceases to exist as one can see by inspecting Fig. 11 for $\epsilon = 0.5$.

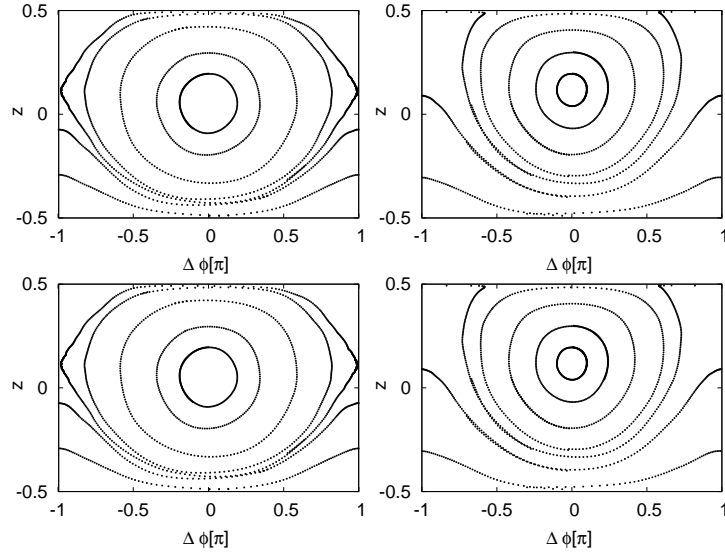


FIG. 11: Phase diagrams for $\epsilon = 0.25$ (left column) and $\epsilon = 0.5$ (right column) and $N = 0.5$. The results from the ordinary differential equations (22)-(23) are shown in the top row, while the corresponding results from the partial differential equation are shown in the bottom row.

A detailed discussion of the dynamical comparison of the two-mode approximation with the corresponding results of the full system can be found in [19]. There, it is highlighted how the effect of a reduced barrier height of the trapping potential or increased interactions can deteriorate the dynamical effectiveness of the two-mode reduction.

Here we explore the role of the collisional inhomogeneity in affecting the accuracy of this reduction, by illustrating a prototypical diagnostic, namely the critical population imbalance threshold beyond which self-trapping occurs, as this is identified in the full dynamical equation and as it is obtained within the two-mode reduction. This is shown in Fig. 12. It can be seen that as ϵ increases, both critical points (the positive and the negative one) increase. The positive one vanishes when it is equal to the total number of atoms. By comparing the results obtained by solving the PDE with the results of the ODEs one observes that the two-mode approximation becomes less accurate, as ϵ increases, in

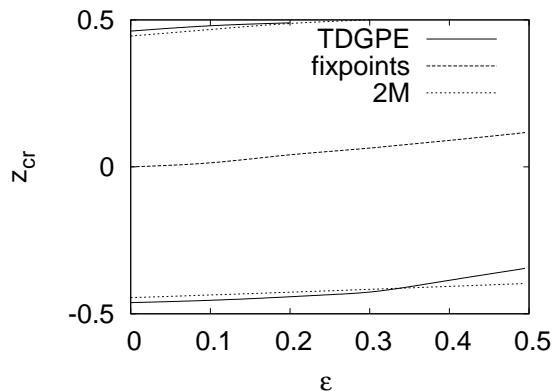


FIG. 12: The critical points z_{cr} of population imbalance above which there exists self-trapping are shown in the time-dependent Gross-Pitaevskii equation (TDGPE) and in the two-mode approximation (2M) for $N = 0.5$. Notice that in this setting, the population imbalance becomes nonzero when $\epsilon \neq 0$ due to the asymmetry (as shown by the dashed line).

capturing the corresponding threshold, a feature that we have also seen regarding stationary state properties; see e.g. Fig. 8.

V. CONCLUSIONS AND OUTLOOK

In this paper, we studied in detail the nature of the most fundamental matter-waves (emanating from the linear limit of the problem) that emerge from a quasi-1D collisionally inhomogeneous Bose-Einstein condensate trapped in a double-well potential. We specifically considered a setup which features distinct scattering lengths between the two wells, including also the case where the nonlinearity coefficient of the pertinent Gross-Pitaevskii equation has different signs in the two wells. We observed that the relevant phenomenology is different in the considered collisionally inhomogeneous environment in comparison to the collisionally homogeneous case studied previously. In particular, even for weak inhomogeneities, the asymmetry (that the spatial dependence of the nonlinearity introduces) induces a modification of the bifurcation picture of the double-well potential and a change in the nature of the symmetry-breaking bifurcation from a pitchfork to a saddle-node; this is reminiscent of similar modifications to the bifurcation picture due to asymmetries of the linear potential [22]. On the other hand, it was found that as the strength of the inhomogeneity is increased, even this saddle-node “recollection” of the symmetry-breaking bifurcation eventually disappears (the corresponding critical point is pushed to infinity) and only one nonlinear branch persists that corresponds to each state of the problem’s linear limit. Interestingly also, as the inhomogeneity acquires opposite sign values of the scattering length, the monotonicity of the number of atoms’ dependence on the chemical potential may change (and may even be different between the two branches), although they do maintain their stability (which presents an interesting deviation –in this spatially inhomogeneous case– from the well-known Vakhitov-Kolokolov criterion that we rationalized in detail above). All of this phenomenology, including the detailed bifurcation diagram and other specific features, such as the critical point of the saddle-node bifurcation and its dependence on the degree of inhomogeneity, are captured remarkably accurately by a Galerkin-type, two-mode approximation and a resulting simple set of algebraic equations. Finally, we also briefly discussed dynamical aspects of the system including a phase space reduction in the population imbalance-interwell phase difference space. We have illustrated that despite the ensuing asymmetry in the phase space (for positive vs. negative population imbalances), the two-mode reduction can accurately capture the threshold of transition from Josephson matter-wave oscillations to nonlinearly induced self-trapping (especially so for weak collisional inhomogeneities).

Our investigation herein presents some testable predictions for the original physical system and its realization in atomic physics or, also possibly, in nonlinear optics [25]; in particular, as the nonlinearity becomes increasingly different in the two wells, the emergence of additional states should be occurring for increasingly larger number of atoms and eventually, such additional states (in particular, the stable one among them) should no longer be observable. It would be of particular interest if such spatial variations of the nonlinearity could be experimentally realized, which would allow the direct testing of our theoretical predictions.

The work of D.J.F. was partially supported by the Special Research Account of the University of Athens. P.G.K.

acknowledges support from NSF-CAREER, NSF-DMS-0505663 and NSF-DMS-0619492.

-
- [1] C. J. Pethick and H. Smith, *Bose-Einstein condensation in dilute gases*, Cambridge University Press (Cambridge, 2002).
- [2] L. P. Pitaevskii and S. Stringari, *Bose-Einstein Condensation*, Oxford University Press (Oxford, 2003).
- [3] K. E. Strecker, G. B. Partridge, A. G. Truscott, and R. G. Hulet, *Nature* **417**, 150 (2002).
- [4] L. Khaykovich, F. Schreck, G. Ferrari, T. Bourdel, J. Cubizolles, L. D. Carr, Y. Castin, and C. Salomon, *Science* **296**, 1290 (2002).
- [5] S. L. Cornish, S. T. Thompson, and C. E. Wieman, *Phys. Rev. Lett.* **96**, 170401 (2006).
- [6] S. Burger, K. Bongs, S. Dettmer, W. Ertmer, K. Sengstock, A. Sanpera, G. V. Shlyapnikov, and M. Lewenstein, *Phys. Rev. Lett.* **83**, 5198 (1999).
- [7] J. Denschlag, J.E. Simsarian, D.L. Feder, C.W. Clark, L.A. Collins, J. Cubizolles, L. Deng, E. W. Hagley, K. Helmerson, W. P. Reinhardt, S. L. Rolston, B. I. Schneider, and W. D. Phillips, *Science* **287**, 97 (2000).
- [8] B. P. Anderson, P. C. Haljan, C. A. Regal, D. L. Feder, L. A. Collins, C. W. Clark, and E. A. Cornell, *Phys. Rev. Lett.* **86**, 2926 (2001).
- [9] Z. Dutton, M. Budde, Ch. Slowe, and L. V. Hau, *Science* **293**, 663 (2001).
- [10] B. Eiermann, Th. Anker, M. Albiez, M. Taglieber, P. Treutlein, K.-P. Marzlin, and M. K. Oberthaler, *Phys. Rev. Lett.* **92**, 230401 (2004).
- [11] P. G. Kevrekidis, D. J. Frantzeskakis, and R. Carretero-González (eds.), *Emergent nonlinear phenomena in Bose-Einstein condensates. Theory and experiment* (Springer-Verlag, Berlin, 2008).
- [12] Yu. S. Kivshar and G. P. Agrawal, *Optical Solitons: From Fibers to Photonic Crystals*, Academic Press (San Diego, 2003).
- [13] D. N. Christodoulides, F. Lederer and Y. Silberberg, *Nature* **424**, 817 (2003); J. W. Fleischer, J. Fleischer, G. Bartal, O. Cohen, T. Schwartz, O. Manela, B. Freedman, M. Segev, H. Buljan, and N. Efremidis, *Opt. Expr.* **13**, 1780 (2005).
- [14] M. Albiez, R. Gati, J. Fölling, S. Hunsmann, M. Cristiani, and M. K. Oberthaler, *Phys. Rev. Lett.* **95**, 010402 (2005).
- [15] S. Raghavan, A. Smerzi, S. Fantoni, and S. R. Shenoy, *Phys. Rev. A* **59**, 620 (1999); S. Raghavan, A. Smerzi and V. M. Kenkre, *Phys. Rev. A* **60**, R1787 (1999); A. Smerzi and S. Raghavan, *Phys. Rev. A* **61**, 063601 (2000).
- [16] E. A. Ostrovskaya, Y. S. Kivshar, M. Lisak, B. Hall, F. Cattani, and D. Anderson, *Phys. Rev. A* **61**, 031601 (R) (2000).
- [17] K. W. Mahmud, J. N. Kutz and W. P. Reinhardt, *Phys. Rev. A* **66**, 063607 (2002).
- [18] V. S. Shchesnovich, B.A. Malomed, and R. A. Kraenkel, *Physica D* **188**, 213 (2004).
- [19] D. Ananikian, and T. Bergeman, *Phys. Rev. A* **73**, 013604 (2006).
- [20] P. Ziñ, E. Infeld, M. Matuszewski, G. Rowlands, and M. Trippenbach, *Phys. Rev. A* **73**, 022105 (2006).
- [21] T. Kapitula and P. G. Kevrekidis, *Nonlinearity* **18**, 2491 (2005).
- [22] G. Theocharis, P. G. Kevrekidis, D. J. Frantzeskakis and P. Schmelcher, *Phys. Rev. E* **74**, 056608 (2006).
- [23] D. R. Dounas-Frazer and L. D. Carr, arXiv:quant-ph/0610166.
- [24] C. Cambournac, T. Sylvestre, H. Maillotte, B. Vanderlinden, P. Kockaert, Ph. Emplit, and M. Haelterman, *Phys. Rev. Lett.* **89**, 083901 (2002).
- [25] P. G. Kevrekidis, Z. Chen, B. A. Malomed, D. J. Frantzeskakis, and M. I. Weinstein, *Phys. Lett. A* **340**, 275 (2005).
- [26] M. Ornigotti, G. Della Valle, D. Gatti, and S. Longhi, *Phys. Rev. A* **76**, 023833 (2007).
- [27] C. Wang, P.G. Kevrekidis, N. Whitaker, and B.A. Malomed, arXiv:0805.0023; *Physica D*, in press (2008).
- [28] Ö.E. Müstecaplioglu, M. Zhang and L. You, *Phys. Rev. A* **71**, 053616 (2005).
- [29] Ö.E. Müstecaplioglu, W. Zhang and L. You, *Phys. Rev. A* **75**, 023605 (2007).
- [30] T. Köhler, K. Goral and P. S. Julienne, *Rev. Mod. Phys.* **78**, 1311 (2006).
- [31] S. Inouye, M. R. Andrews, J. Stenger, H. J. Miesner, D. M. Stamper-Kurn and W. Ketterle, *Nature* **392**, 151 (1998); J. Stenger, S. Inouye, M. R. Andrews, H.-J. Miesner, D. M. Stamper-Kurn, and W. Ketterle, *Phys. Rev. Lett.* **82**, 2422 (1999); J. L. Roberts, N. R. Claussen, J. P. Burke Jr., C. H. Greene, E. A. Cornell, and C. E. Wieman, *Phys. Rev. Lett.* **81**, 5109 (1998); S. L. Cornish, N. R. Claussen, J. L. Roberts, E. A. Cornell, and C. E. Wieman, *Phys. Rev. Lett.* **85**, 1795 (2000).
- [32] F. K. Fatemi, K. M. Jones, and P. D. Lett, *Phys. Rev. Lett.* **85**, 4462 (2000); M. Theis, G. Thalhammer, K. Winkler, M. Hellwig, G. Ruff, R. Grimm, and J. H. Denschlag, *Phys. Rev. Lett.* **93**, 123001 (2004).
- [33] J. Herbig, T. Kraemer, M. Mark, T. Weber, C. Chin, H. C. Nagerl, and R. Grimm, *Science* **301**, 1510 (2003); C. A. Regal, C. Ticknor, J. L. Bohn, and D. S. Jin, *Nature* **424**, 47 (2003).
- [34] M. Bartenstein, A. Altmeyer, S. Riedl, S. Jochim, C. Chin, J. H. Denschlag, and R. Grimm, *Phys. Rev. Lett.* **92**, 203201 (2004); T. Bourdel, L. Khaykovich, J. Cubizolles, J. Zhang, F. Chevy, M. Teichmann, L. Tarruell, S.J.J.M.F. Kokkelmans, and C. Salomon, *Phys. Rev. Lett.* **93**, 050401 (2004).
- [35] F. Kh. Abdullaev, J. G. Caputo, R. A. Kraenkel, and B. A. Malomed, *Phys. Rev. A* **67**, 013605 (2003); H. Saito and M. Ueda, *Phys. Rev. Lett.* **90**, 040403 (2003); G. D. Montesinos, V. M. Pérez-García, and P. J. Torres, *Physica D* **191** 193 (2004).
- [36] P. G. Kevrekidis, G. Theocharis, D. J. Frantzeskakis, and B. A. Malomed, *Phys. Rev. Lett.* **90**, 230401 (2003); D. E. Pelinovsky, P. G. Kevrekidis, and D. J. Frantzeskakis, *Phys. Rev. Lett.* **91**, 240201 (2003); D. E. Pelinovsky, P. G. Kevrekidis, D. J. Frantzeskakis, and V. Zharnitsky, *Phys. Rev. E* **70**, 047604 (2004); Z. X. Liang, Z. D. Zhang, and W. M. Liu, *Phys. Rev. Lett.* **94**, 050402 (2005); M. Matuszewski, E. Infeld, B. A. Malomed, and M. Trippenbach, *Phys. Rev.*

Lett. **95**, 050403 (2005).

- [37] G. Theoharis, P. Schmelcher, P. G. Kevrekidis and D. J. Frantzeskakis, Phys. Rev. A **72**, 033614 (2005).
- [38] F.Kh. Abdullaev and M. Salerno, J. Phys. B **36**, 2851 (2003).
- [39] M. I. Rodas-Verde, H. Michinel, and V. M. Pérez-García, Phys. Rev. Lett. **95**, 153903 (2005); A. V. Carpenter, H. Michinel, M. I. Rodas-Verde, and V. M. Pérez-García, Phys. Rev. A **74**, 013619 (2006).
- [40] G. Theoharis, P. Schmelcher, P. G. Kevrekidis and D. J. Frantzeskakis, Phys. Rev. A **74**, 053614 (2006).
- [41] F.Kh. Abdullaev, and J. Garnier, Phys. Rev. A **74**, 013604 (2006).
- [42] G. Dong, B. Hu, and W. Lu, Phys. Rev. A **74**, 063601 (2006).
- [43] Yu. V. Bludov, V. A. Brazhnyi, and V. V. Konotop, Phys. Rev. A **76**, 023603 (2007).
- [44] P. Niarchou, G. Theoharis, P. G. Kevrekidis, P. Schmelcher, and D. J. Frantzeskakis, Phys. Rev. A **76**, 023615 (2007).
- [45] F. Kh. Abdullaev and J. Garnier, Phys. Rev. A **72**, 061605(R) (2005).
- [46] H. Sakaguchi and B. A. Malomed, Phys. Rev. E **72**, 046610 (2005); M. A. Porter, P. G. Kevrekidis, B. A. Malomed, and D. J. Frantzeskakis, Physica D **229**, 104 (2007); F. Kh. Abdullaev, A. Abdumalikov and R. Galimzyanov, Phys. Lett. A **367**, 149 (2007).
- [47] Y. Bludov and V. V. Konotop, Phys. Rev. A **74**, 043616 (2006).
- [48] M. T. Primatarowa, K. T. Stoychev and R. S. Kamburova, Phys. Rev. E **72**, 036608 (2005).
- [49] V. M. Pérez-García, arXiv:nlin/0612028.
- [50] G. Fibich, Y. Sivan, and M. I. Weinstein, Physica D **217**, 31 (2006).
- [51] Y. Sivan, G. Fibich, and M. I. Weinstein, Phys. Rev. Lett. **97**, 193902 (2006);
- [52] J. Belmonte-Beitia, V. M. Pérez-García, V. Vekslerchik, and P. J. Torres, Phys. Rev. Lett. **98**, 064102 (2007).
- [53] Z. Rapti, P. G. Kevrekidis, V. V. Konotop and C. K. R. T. Jones, J. Phys. A: Math. Theor. **40**, 14151 (2007).
- [54] F. Kh. Abdullaev, Yu. V. Bludov, S. V. Dmitriev, P. G. Kevrekidis and V. V. Konotop, Phys. Rev. E **77**, 016604 (2008).
- [55] A. S. Rodrigues, P. G. Kevrekidis, M. A. Porter, D.J. Frantzeskakis, P. Schmelcher, and A. R. Bishop, arXiv:0712.0986.
- [56] P. Krueger, personal communication.
- [57] V. M. Pérez-García, H. Michinel, and H. Herrero, Phys. Rev. A **57**, 3837 (1998); A. D. Jackson, G. M. Kavoulakis, and C. J. Pethick, Phys. Rev. A **58**, 2417 (1998).
- [58] T. Kapitula and P.G. Kevrekidis, Chaos **15**, 037114 (2005).
- [59] N. G. Vakhitov and A. A. Kolokolov, Radiophys. Quantum Electron. **16**, 783 (1973).
- [60] I. M. Merhasin, B. V. Gisin, R. Driben and B. A. Malomed, Phys. Rev. E **71**, 016613 (2005).
- [61] M.G. Grillakis, Comm. Pure Appl. Math. **41**, 747 (1988); M.G. Grillakis, J. Shatah and W.A. Strauss, J. Funct. Anal. **74**, 160 (1987).
- [62] J. Gomez-Gardenes, B.A. Malomed, L.M. Floría and A.R. Bishop, Phys. Rev. E **73**, 036608 (2006).
- [63] We note in passing that for the multi-component system the diagram is also substantially different (in that case, more involved) than that of the single component one, due to the presence of “mixed states”, mixing the symmetric and anti-symmetric nonlinear states of *each* of the two components (and bifurcations thereof).